Journal of Computational Physics 228 (2009) 2313–2333

Contents lists available at ScienceDirect

Journal of Computational Physics

journal homepage: www.elsevier.com/locate/jcp

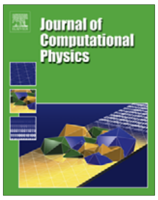

Perspective on the geometric conservation law and finite element methods for ALE simulations of incompressible flow

S. Étienne *, A. Garon, D. Pelletier

École Polytechnique de Montréal, Mechanical Engineering Department, C.P. 6079, Succ. Center-Ville, Montreal, Quebec, Canada H3C3A7

ARTICLE INFO

Article history:
Received 25 June 2008
Received in revised form 18 November 2008
Accepted 21 November 2008
Available online 13 December 2008

Keywords:
Arbitrary Lagragian Eulerian
Finite element method
Geometric conservation law
High order time integrators
Navier–Stokes equations
Incompressible flow simulations

ABSTRACT

This paper takes a fresh look at the geometric conservation law (GCL) from the perspective of the finite element method (FEM) for incompressible flows. The GCL arises naturally in the context of Arbitrary Lagrangian Eulerian (ALE) formulations for solving problems on deforming domains. GCL compliance is traditionally interpreted as a consistency criterion for applying an unsteady flow solution algorithm to simulate exactly a uniform flow on a deforming domain. We introduce an additional requirement: the time integrator must maintain its fixed mesh accuracy when applied to deforming meshes. A review of the literature shows that while many authors use an ALE FEM, few of them discuss the GCL issues. We show how a fixed mesh unsteady FEM using high order time integrator (up to fifth order in time) can be transposed to solve problems on deforming meshes and preserve its fixed mesh high order temporal accuracy. An appropriate construction of the divergence of the mesh velocity guarantees GCL compliance while a separate construction of the mesh velocity itself allows the time-integrator to deliver its fixed mesh high order temporal accuracy on deforming domains. Analytical error analysis of problems with closed form solutions provides insight on the behavior of the time integrators. It also explains why high order temporal accuracy is achieved with a conservative formulation of the incompressible Navier–Stokes equations, while only first order time accuracy is observed with the non-conservative formulation and all time-integrators investigated here. We present thorough time-step and grid refinement studies for simple problems with closed form solutions and for a manufactured solution with a non-trivial flow on a deforming mesh. In all cases studied, the proposed reconstructions of the mesh velocity and its divergence for the conservative formulation lead to optimal time accuracy on deforming grids.

1. Introduction

Arbitrary Lagrangian Eulerian (ALE) formulations are very popular for solving differential equations on deforming domains. In this approach the partial differential equations (PDE's), here the unsteady Navier–Stokes equations, are expressed with respect to a reference fixed configuration. A so-called ALE mapping associates at each time t a point in the current computational domain $\Omega(t)$ to a point in the reference domain $\Omega(0)$. This ensures that the solution evolves along trajectories that are contained in the computational domain at all times. When discussing ALE formulations, several issues are raised by different authors. What is the regularity of the mapping required to ensure that the problem is well posed? How is the mapping defined, represented and discretized? What is the effect of the mesh velocity on the accuracy on the time integrator? What is

* Corresponding author. Tel.: +1 52143404711x5897; fax: +1 3405917.
E-mail address: stephane.etienne@polymtl.ca (S. Étienne).

0021-9991/$ - see front matter © 2008 Elsevier Inc. All rights reserved.
doi:10.1016/j.jcp.2008.11.032

the level of stability of the resulting algorithm? The bulk of these issues is usually discussed in the context of the GCL or geometric conservation law [1].

This paper takes a fresh look at the GCL from the somewhat restricted perspective of finite element methods for incompressible flows, using the usual definitions of the GCL and its discrete counterpart. However these definitions do not address the issues raised in the previous paragraph about the interactions between the mesh motion, its discretisation and that of space and time discretisation schemes, especially its time accuracy. As we will show, a poor choice of a single component of the ALE formulation results in a lower accuracy on deforming domains than that observed on fixed domains.

1.1. Literature review

The GCL has been the subject of many investigations and has generated several controversial opinions. It is generally accepted that if an ALE formulation preserves a uniform flow on a deforming grid, then this constitutes either a definition of the GCL or a GCL compliance test for the numerical scheme [2–8]. For instance Shyy et al. [9] demonstrated that without explicitly enforcing the GCL, $O(1)$ errors could be induced in the computations due solely to grid movement effects. Thus, it appears that GCL compliance may have a significant effect on the performance of an ALE scheme.

The space–time finite element method (STFEM), an alternative to ALE Methods, has received much attention because in the case of the STFEM the GCL issue disappears completely. However this comes at the cost of doubling the number of unknowns at each time-step for a second order time-stepping scheme. Thus there remains much interest in ALE schemes because of their lower computational expense. STFEM have been developed by many authors such as N'dri et al. [10] for Computational Fluid Dynamics, Li et al. [11] for Structural Dynamics, and Hansbo et al. [12], Stein et al. [13] for Fluid–Structure Interaction problems.

GCL compliance, or how the ALE mesh velocity is computed, often appears as a necessary condition for consistency of an ALE numerical scheme. Lacroix et al. [14] showed that many simple techniques work well for unidirectional mesh motions. However, many schemes reveal their limitations as soon as arbitrary 2D mesh motions are considered. Lesoinne and Farhat [4] state that compliance can be tested by verifying satisfaction of the discrete version of the GCL. That is checking that a uniform flow is not polluted by approximation errors caused by mesh motion.

Table 1 shows a compilation of many contributions and approaches to the GCL. All but one are concerned with time integrators of order 1 or 2. Mavriplis [26] discusses the construction of GCL compliant Finite Volume formulations for time-stepping schemes of order higher than 2. Thus, there is a definite need to investigate how to develop GCL compliant ALE FEM with high order temporal accuracy. The fifth column in Table 1 indicates the order of convergence in space and time of the schemes used in each paper. The next to last column of the table indicates whether or not systematic time step refinement studies were performed by the authors. Several authors show results with such complex geometries or flow physics that it most likely masks the effects of GCL compliance. In such situations, we consider that convergence studies are inconclusive even when they have been performed. The last column indicates if a theoretical stability analysis has been performed.

Previous studies used various names and acronyms to refer to different aspects of the GCL. The concept of GCL was first introduced in 1961 by Trulio et al. [1] and later generalized by Thomas et al. [15] for the finite volume method (FVM).

Table 1
Methods (FE: finite element, FD: finite difference, FV: finite volume), formulation of PDE's (C: conservative, NC: non-conservative), discretisation order, occurrence of grid convergence and stability study and Incompressible flows study.

Author	Year	Method	Form.	Order	Grid Conv.	Stability study	Inc.
Trulio [1]	1961	FD	C	–	–	–	–
Thomas [15]	1979	FD	C	$\Delta x^2, \Delta t$	–	–	–
Demirdzic [16]	1988	FV	C	–	Yes	–	–
Lacroix [14]	1992	FD	C	$\Delta x^2, \Delta t$	–	–	Yes
Zhang [8]	1993	FV/FD	C	$\Delta x^2, \Delta t$	–	–	–
Lesoinne [4]	1996	FV/FE	C	Δt^2	–	–	–
Formaggia [17]	1999	FE	C/NC	Δt^2	–	Yes	–
Koobus [7]	1999	FV/FE	C	$\Delta x^2, \Delta t^2$	–	–	–
Guillard [5]	2000	FV	C	$\Delta x^2, \Delta t^2$	–	–	–
Nkonga [18]	2000	FE	C	Δt^3	–	–	–
Farhat [19]	2001	FV	C	$\Delta x^2, \Delta t^2$	–	Yes	–
Cao [20]	2002	FV	C	Δt^2	–	–	–
Kamakoti [6]	2003	FV	C	$\Delta t, \Delta t^2$	Yes	–	–
Gordnier [21]	2003	FD	C	Δt	–	–	–
Lian [22]	2003	FV	C	–	–	–	Yes
Boffi [23]	2004	FE	C	$\Delta x^2, \Delta t^2$	Yes	Yes	–
Formaggia [3]	2004	FE	C/NC	Δt^2	Yes	Yes	–
Jan [24]	2004	FE	C	–	–	–	Yes
Geuzaine [25]	2003	FV	C	Δt^2	Yes	–	–
Mavriplis [26]	2005	FV	C	$\Delta x^2, \Delta t^4$	Yes	–	–
Engel [27]	2005	FV	C	–	Yes	–	
Förster [28]	2006	FE	C	$\Delta x^2, \Delta t^2$	Yes	–	Yes
Present	2008	FE	C/NC	$\Delta x^3, \Delta t^5$	Yes	–	Yes

Different approaches have been considered. As observed by Demirdžic et al. [16], the true significance of the Space Conservation Law (SCL) or GCL, was probably not recognized initially because most studies were performed with one-dimensional mesh motions for which it is much easier to satisfy the GCL, than on grids subjected to arbitrary motion. This is why many highly successful 1D schemes failed when generalised to two or three dimensions. Förster et al. [28] showed that a simple formula can be used to compute the mesh velocity for 1D grid motions. However, since they do not show results for more general 2D grid motions, it cannot be inferred that their formulation satisfies the GCL in 2D or 3D.

Much of initial work on the GCL was performed using finite volume methods. While the FVM and FEM often lead to identical schemes in 1D, multi-dimensional discretisations of fluid flow equations result in different computational stencils. Hence, one can legitimately expect that an effective finite volume ALE technique might not apply directly to finite element discretisations without some adjustments.

Zhang et al. [8] discussed previous studies and their limitations with regards to general purpose application. They note that a numerical scheme is said to satisfy the Volume Conservation Law (VCL) if it guarantees satisfaction of both the continuity equation and the SCL for a uniform flow. They stress that satisfying these two laws is required to satisfy the GCL.

1.2. DGCL and temporal accuracy

The discrete geometric conservation law (DGCL) of Farhat et al. [19] provides significant insight on the accuracy of the time-stepping scheme. For a pth order time-accurate scheme ($p \geqslant 1$) on a fixed mesh, satisfying the discrete geometric conservation law to pth order accuracy is a sufficient condition for this scheme to be at least first order time-accurate on a moving mesh [5], meaning that in practice the time accuracy of a DGCL compliant scheme might be reduced from pth order on a fixed mesh to as low as first order on a deforming mesh. Also, the higher the order of a time-stepping scheme on a fixed grid, the more important it becomes for this scheme to satisfy the DGCL for successful applications to flows on a moving grid. Furthermore, unless restricted by numerical stability conditions, a numerical method satisfying the DGCL will generally allow a much larger computational time-step than its counterpart violating the DGCL.

Mavriplis et al. [26] as well as Geuzaine et al. [25] showed that it is possible to construct an ALE formulation which preserves the fixed mesh temporal accuracy of the time-stepping scheme on a deforming mesh without satisfying the DGCL. Furthermore, Mavriplis also states that the DGCL is unrelated to the time-accuracy! Geuzaine et al. [25], have proven that the DGCL is neither a necessary nor a sufficient condition to preserve time-accuracy.

1.3. DGCL and stability

The effect of GCL on stability of ALE Methods is controversial. This question is still open for debate as shown by the opposing conclusions of Farhat et al. [19] and Boffi et al. [23]. In the paper by Farhat the DGCL appears as a necessary and sufficient condition for stability of schemes with up to 2nd order temporal accuracy, while Boffi et al. [23] and Formaggia and Nobile [3] showed that it is neither necessary nor sufficient for stability except for the 1st order backward Euler Implicit scheme. They conclude that GCL compliance is likely to improve accuracy of the numerical scheme and enhance its stability in some cases.

Mavriplis compared non-DGCL-compliant to DGCL-compliant schemes of the same temporal accuracy [26]. The latter ones appear to be free from oscillations that are unavoidable in the former ones. He attributed these oscillations to the lack of conservation induced by violation of the GCL. In [19], Farhat et al. showed too that schemes violating the DGCL while generating accurate solutions, were polluted by bounded oscillations whereas those satisfying the DGCL did not exhibit spurious oscillations. Numerical consistency requires satisfaction of the geometric conservation law (GCL) to avoid spurious solutions.

Kamakoti et al. [6] present an unusual approach. The flow field is advanced in time to t^{n+1} using the implicit Euler scheme while a GCL compliant mesh velocity field is obtained at t^{n+1} with variants of first or second order implicit time-integrators. They found that the best results are obtained when the first order implicit Euler scheme is applied to both the flow and mesh velocity.

1.4. Approaches to the GCL

There are several ways to achieve GCL compliance. Formaggia and Nobile [3] take the following approach to the GCL. Given a spatial discretisation of a convection–diffusion equation and an ALE mapping (mesh velocity), they seek variants of a given time integrator such that the GCL is satisfied. Their approach involves multi-point time quadrature of the right-hand side of the systems of ODE's in time. For instance, for solving $dy/dt = g(t, u(t))$ they replace the standard implicit backward Euler

$$y^{n+1} - y = \Delta t g(t^{n+1}, u^{n+1}(t)) \tag{1}$$

by the following modified scheme

$$y^{n+1} - y^n = \Delta t \sum_{l=0}^{m} w_l g(t^l, u^{n+1}(t)) \tag{2}$$

This involves $m+1$ evaluations of the PDE residuals, an expensive proposal for large finite element problems. Such an approach has also been chosen in [4,25], for example. Interestingly, Lesoinne and Farhat [4] adopt a similar philosophy. Their 2D GCL compliant FV scheme uses the trapezoidal rule for evaluating the mesh velocity. In 3D, they use the 3D analog of their 2D Finite Volume discretisation of space but replace the Crank–Nicholson time integrator by a n-step multipoint time integrator similar to that expressed by formula (2).

1.5. The present work

We take a different approach: given a spatial discretisation and a time-integrator, we seek a method for evaluating the divergence of the mesh velocity to satisfy the GCL, and a second method to compute the mesh velocity so as to ensure that high temporal accuracy observed on fixed meshes is maintained on moving meshes. In a sense we separate the computation of the mesh velocity and that of its divergence as if they arose from two distinct mesh velocity fields. We believe that this approach offers several advantages. Code development and implementation are simplified as the time integrator routine remains unchanged. In fact, the same routine is used in 2D and 3D and for fixed and deforming meshes. Modifications are confined to a handful of routines for evaluation of the weak form residuals, mesh velocity divergence, and mesh velocity itself. Thus development time is reduced. Code maintenance is simplified since there is no need to maintain separate integrators for fixed mesh and deforming mesh simulations nor is there requirement to use different integrators in 2D/3D simulations. Finally, because identical integrators are used in all cases, analysis of results, and diagnosis of odd simulation results are also simplified.

Furthermore, incompressible flows present an additional difficulty. Because pressure acts as the Lagrange multiplier enforcing the incompressibility constraint (continuity equation), achieving higher order time accuracy for pressure is more difficult in incompressible flows than in compressible flows. In fact, for time-stepping schemes of order greater than 2 for the velocity, incompressibility is achieved at the cost of a reduction of the temporal accuracy in pressure. In this study, we consider the Crank–Nicholson (2nd order for velocity and pressure) and a family of fully implicit Runge–Kutta schemes that are 3rd and 5th order time accurate for velocity and 2nd and 3rd order time accurate for pressure.

To shed some light we propose testing the GCL at three levels of compliance:

(1) *GCL level 1*: an Arbitrary Lagrangian Eulerian (ALE) formulation satisfying the GCL must produce the exact solution to the no-flow test on arbitrary deforming grids (see [16]).
(2) *GCL level 2*: an ALE formulation satisfying the GCL must produce the exact solution of a uniform flow on moving grids, this is the so-called Discrete GCL (DGCL) by Farhat et al. [19].
(3) *GCL level 3*: for a properly designed ALE formulation satisfying the GCL, the time-stepping scheme must exhibit the same convergence rate on deforming and fixed grids [19,26].

The first two levels are commonly found in the literature. The third one is a powerful test of time integrators, especially high order ones.

We show through carefully chosen examples that satisfying the constant solution test on a moving grid, *i.e.* the usual standard GCL compliance test, does not guarantee that the high order temporal accuracy observed on fixed meshes will also occur on moving meshes.

This paper is organized as follows. Section 2 describes the governing equations for laminar flows of incompressible fluids on deforming domains. This is followed by a brief overview of the finite element method used to solve the equations. Section 4 discusses the conservative and non-conservative weak forms of the ALE problems The next section provides a general framework useful to compare time-integrators. Section 6 is a detailed development of methods to evaluate the mesh velocity divergence so as to satisfy the GCL. The separate construction of the mesh velocity itself to achieve high order temporal accuracy is the subject of Section 7. Section 8 presents results from careful numerical tests and analytical error analysis. Sections 9 and 10 present a discussion of the results and conclusions.

2. Governing equations

The flow of an incompressible fluid is described by the continuity and momentum equations [29] written in *convective* (non-conservative) form

$$\nabla \cdot \mathbf{u} = 0 \tag{3}$$

$$\rho \mathbf{u}_{,t} + \rho(\mathbf{u} \cdot \nabla)\mathbf{u} = \nabla \cdot \boldsymbol{\sigma} + \mathbf{f} \tag{4}$$

In an arbitrary time-dependent coordinate system, the momentum equations (4) are written, in non-conservative form as

$$\rho \mathbf{u}_{,t} + \rho[(\mathbf{u} - \mathbf{v}) \cdot \nabla]\mathbf{u} = \nabla \cdot \boldsymbol{\sigma} + \mathbf{f} \tag{5}$$

where $\mathbf{v}$ is the velocity of the moving reference frame, ρ the fluid density, $\mathbf{u}$ the fluid velocity, $\boldsymbol{\sigma}$ the total fluid stress tensor (pressure and viscous forces), and $\mathbf{f}$ a body force. Eqs. (3) and (4) are expressed in an Eulerian frame of reference while Eq. (5) is expressed in an Arbitrary Lagrangian Eulerian (ALE) coordinate system. Details of its development can be found in [14]. Assuming that the fluid is Newtonian, its constitutive equation is given by

$$\boldsymbol{\sigma} = \boldsymbol{\tau} - p\mathbf{I} \quad \text{with } \boldsymbol{\tau} = \mu[\nabla\mathbf{u} + (\nabla\mathbf{u})^T]$$

where μ is the dynamic viscosity and p is the fluid pressure. The flow equations are closed with the following boundary conditions,

$$\begin{aligned} \boldsymbol{\sigma}\cdot\mathbf{n} &= \bar{\mathbf{t}} \quad \text{on } \Gamma_N \\ \mathbf{u} &= \bar{\mathbf{u}} \quad \text{on } \Gamma_D \end{aligned} \tag{6}$$

where Γ_N denotes a boundary where Neumann conditions are applied in the form of prescribed surface forces (tractions) $\bar{\mathbf{t}}$, and Γ_D corresponds to a Dirichlet boundary on which the velocity, $\bar{\mathbf{u}}$, is imposed.

There remains the issue of how to generate and control the grid motion and mesh velocities, *i.e.* manage the domain deformation. This can be done in several ways which only affect the ability of the solver to cope with more or less complicated domain deformations and mesh motions[30,2,31–37,13,38,39]. This issue has no effect on the GCL. We have opted to implement mesh control with the pseudo-solid approach of Sackinger [32] because it allows for a fully coupled continuum formulation. The pseudo-solid model provides physics-based rules using elasticity equations to describe the deformation of the time-varying domain. These equations are fully coupled to the Navier–Stokes equations on the deforming domain.

Recall that in ALE formulations the Navier–Stokes equations are expressed in a non-deformed configuration and that a mapping associates, at each time t, a point in the current deformed domain $\Omega(t)$ to a point in the reference domain $\Omega(0)$. Given that a pseudo-solid approach is used to define the mapping and that the coupled system of PDE's will be solved by a finite element method, it is reasonable to construct the mapping in a piecewise continuous manner with the same finite element basis functions used to represent the geometry of each element in the mesh. Furthermore, it is customary in unstructured meshes of triangles or tetrahedra to use piecewise linear basis functions for the geometry so that the determinant of the Jacobian for the element mapping is constant, *i.e.* assume straight-sided elements.

3. Solution strategy

We have chosen a monolithic solution strategy coupling all degrees of freedom: velocities, pressure, along with pseudo-solid displacements. In this approach all equations are treated implicitly in the time integration scheme. This methodology is applicable not only for flows on deforming meshes but also to fully implicit monolithic treatment of unsteady Fluid–Structure Interactions. Linearisation of the flow and mesh equations must account for all implicit dependencies to ensure quadratic convergence of Newton's method [40]. These steps are implemented simply and in a straight forward manner through the use of numerical Jacobians. This approach is very robust and applicable to a broad spectrum of problems. Note however that the details of the finite element flow solver have no effect on GCL compliance.

The fluid velocity and displacement fields are discretized using 6-noded quadratic elements. Fluid pressure is discretized by piecewise linear continuous functions. This discretisation proves to be useful in our study because all linear and quadratic flows are captured exactly (Couette and Poiseuille, for instance) so that the spatial error is zero leaving time discretisation as the sole contributor to error. In such cases, diagnosis of the temporal order of accuracy becomes easy. The resulting sparse matrix system is solved using the PARDISO software [41,42].

4. Integral formulations and the geometric conservation law

We focus on two weak formulations of the equations. The first one corresponds to the non-conservative form of the Navier–Stokes equations, Eq. (5), and is obtained by multiplying Eq. (5) by a test function $\mathbf{w}$ and integrating over the time varying domain $\Omega(t)$. This means that the non-conservative formulation reads

$$\int_{\Omega(t)} \mathbf{w}\cdot\rho\frac{\partial\mathbf{u}}{\partial t}d\Omega + \int_{\Omega(t)} \mathbf{w}\cdot\{\rho[(\mathbf{u}-\mathbf{v})\cdot\nabla]\mathbf{u} + \nabla\mathbf{w}:\boldsymbol{\sigma}\}d\Omega = \int_{\Gamma_N(t)} \mathbf{w}\cdot(\boldsymbol{\sigma}\cdot\mathbf{n})d\Gamma \tag{7}$$

Note that we consider transformation $T^{(t)}$ from $\Omega(0)$ to $\Omega(t)$ to be regular at all times, *i.e.* of class $C^{(1)}$, univalent and such that $J(t)T^{(t)}\neq 0$ on $\Omega(0)$. $J(t)$ is the determinant of the Jacobian of the transformation from $\Omega(0)$, the reference domain, to $\Omega(t)$, the domain

Proposition 1. *We can reformulate Eq. (7) to obtain the following conservative formulation*

$$\frac{d}{dt}\int_{\Omega(t)} \mathbf{w}\cdot\rho\mathbf{u}d\Omega - \int_{\Omega(t)} \mathbf{w}\cdot(\nabla\cdot\mathbf{v})\rho\mathbf{u}d\Omega + \int_{\Omega(t)} \mathbf{w}\cdot\{\rho[(\mathbf{u}-\mathbf{v})\cdot\nabla]\mathbf{u} + \nabla\mathbf{w}:\boldsymbol{\sigma}\}d\Omega = \int_{\Gamma_N(t)} \mathbf{w}\cdot(\boldsymbol{\sigma}\cdot\mathbf{n})d\Gamma \tag{8}$$

Proof 1. Using the temporal derivative of J expressed in terms of the mesh velocity $\mathbf{v}$ as

$$\frac{\partial J}{\partial t} = J(\nabla \cdot \mathbf{v}) \tag{9}$$

and the fact that test functions and the fluid density do not depend on time when expressed on $\Omega(0)$ leads to the result. □

Eqs. (7) and (8) are, respectively, the non-conservative and the conservative weak formulations. They are strictly equivalent to the Galerkin formulation when the grid is fixed. They are also equivalent to each other in the continuum. The difference lies in the structure of the temporal derivative term which has an effect on GCL compliance at levels 1 and 2. For instance, consider the uniform flow test for GCL compliance, then $\nabla \mathbf{u} = 0$. In the case of Eq. (7) the mesh velocity drops out and does not affect GCL compliance. It turns out that Eq. (7) always complies with the levels 1 and 2 of the GCL. For more complex velocity fields, the mesh velocity will not drop out of Eq. (7) so that ALE predictions using the non-conservative form will depend on the construction of $\mathbf{v}$.

In the case of the conservative form, Eq. (8), the time derivative is applied to the momentum integral and is representative of the fact that the domain of integration also depends on time. For this formulation, the mesh velocity divergence must be evaluated in such a way that the GCL compliance is satisfied.

5. Time-stepping schemes considered

We study three time integration schemes to assess their interactions with the weak forms, Eq. (7) or (8) and their effects on the predictions. We consider the Crank–Nicholson and the 3rd and 5th order Radau IIA schemes. These implicit Runge–Kutta schemes are 2nd, 3rd and 5th order accurate for velocity and 2^{nd}, 2^{nd} and 3^{rd} order accurate for the pressure, respectively (see [43]).

To better appreciate the effects of the time-stepping scheme, we first illustrate their use on the sample ODE $y' = \phi(t, y)$. A general RK scheme applied to this equation reads

$$y_*^{(n+c_i)} = y^{(n)} + \Delta t \sum_{j=1}^{s} a_{ij}\phi(t^{(n+c_j)}, y_*^{(n+c_j)}) \qquad \text{for } i = 1, \ldots, s \tag{10}$$

$$y^{(n+1)} = y^{(n)} + \Delta t \sum_{j=1}^{s} b_j\phi(t^{(n+c_j)}, y_*^{(n+c_j)}) \tag{11}$$

where $t^{(n+c_j)}$ means $t^{(n)} + c_j\Delta t$. This system is summarized compactly in the form of a general Butcher Tableau

$$\begin{array}{c|ccc}
c_1 & a_{11} & \ldots & a_{1s} \\
\vdots & \vdots & \ddots & \vdots \\
c_s & a_{s1} & \ldots & a_{ss} \\
\hline
 & b_1 & \ldots & b_s
\end{array}$$

Following [43], for the three schemes, we have $a_{si} = b_i$, for $i = 1, \ldots, s$ to ensure L-stability so that the projection step defined by Eq. (11) can be skipped. Note also that the RK schemes are constructed to have the following property $c_i = \sum_{k=1}^{s} a_{ik}$, for $i = 1, \ldots, s$.

The Crank–Nicholson time-stepping scheme is of Lobatto IIIa type and is 2nd order accurate for both velocity and pressure. Its Butcher Tableau is

$$\begin{array}{c|ccl}
0 & 0 & 0 & \leftarrow \text{explicit step} \\
1 & 1/2 & 1/2 & \\
\hline
\text{Crank-Nicholson} & 1/2 & 1/2 &
\end{array}$$

The first row corresponds to an explicit step so that we can write the 2-step RK scheme in a single line as

$$y^{(n+1)} = y^{(n)} + \frac{\Delta t}{2}\phi(t^{(n)}, y^{(n)}) + \frac{\Delta t}{2}\phi(t^{(n+1)} + \Delta t, y^{(n+1)}) \tag{12}$$

For incompressible flows, the 3rd and 5th order Radau IIA schemes deliver the expected 3rd and 5th order time accuracy on velocity and only 2nd and 3rd order time accuracy for pressure. According to Hairer et al. [43], because the pressure is a Lagrange multiplier for incompressibility, the Navier–Stokes equations for incompressible flows are a system of index 2 Differential Algebraic Equations which implies a lower time accuracy for the pressure. The Butcher Tableaus of these two schemes are as follows

1/3	5/12	-1/12
1	3/4	1/4
IRK3	3/4	1/4

which translates to

$$y^{(n+1/3)} = y^{(n)} + \frac{5\Delta t}{12}\phi(t^{(n+1/3)}, y^{(n+1/3)}) - \frac{\Delta t}{12}\phi(t^{(n+1)}, y^{(n+1)}) \quad (13)$$

$$y^{(n+1)} = y^{(n)} + \frac{3\Delta t}{4}\phi(t^{(n+1/3)}, y^{(n+1/3)}) + \frac{\Delta t}{4}\phi(t^{(n+1)}, y^{(n+1)}) \quad (14)$$

and means that the two implicit steps are coupled. Thus, doubling the number of unknown when advancing from $t^{(n)}$ to $t^{(n+1)}$ compared to CN. Finally, the Radau IIA5 can be summarized as

$(4-\sqrt{6})/10$	$(88-7\sqrt{6})/360$	$(296-169\sqrt{6})/1800$	$(-2+3\sqrt{6})/225$
$(4+\sqrt{6})/10$	$(296+169\sqrt{6})/1800$	$(88+7\sqrt{6})/360$	$(-2-3\sqrt{6})/225$
1	$(16-\sqrt{6})/36$	$(16+\sqrt{6})/36$	1/9
IRK5	$(16-\sqrt{6})/36$	$(16+\sqrt{6})/36$	1/9

which translates to

$$y^{(n+c_1)} = y^{(n)} + \sum_{j=1}^{3} a_{1j}\Delta t\phi(t^{(n+c_j)}, y^{(n+c_j)}) \quad (15)$$

$$y^{(n+c_2)} = y^{(n)} + \sum_{j=1}^{3} a_{2j}\Delta t\phi(t^{(n+c_j)}, y^{(n+c_j)}) \quad (16)$$

$$y^{(n+c_3)} = y^{(n)} + \sum_{j=1}^{3} a_{3j}\Delta t\phi(t^{(n+c_j)}, y^{(n+c_1)}) \quad (17)$$

which leads to three coupled implicit steps thus tripling the number of unknowns compared to CN.

6. Evaluating the mesh velocity divergence

The objective of this section is to develop systematic constructions of the mesh velocity divergence so as to achieve GCL compliance for the conservative weak form equation (8).

From here on we assume that space has been discretized by a suitable finite element method with straight-sided triangles or tetrahedra which implies that the mesh motion and the mesh velocity are piecewise linear functions of space. The fluid velocity and pressure are discretized with a suitable finite element scheme. We chose the Taylor–Hood element or P2–P1 element for which velocity is discretized with quadratic polynomials and pressure approximated by linear polynomials. This element is 2nd order accurate for the velocity in H^1 norm and 2^{nd} order accurate for the pressure in L_2 norm.

The uniform flow test provides a rule for calculating the divergence of the mesh velocity, $(\nabla \cdot \mathbf{v})$, to satisfy the GCL for the conservative formulation equation (8). As this is done at the discrete level, it is referred to as the DGCL. This implies compliance at levels 1 and 2 by both formulations Eqs. (7) and (8), see Section 4. Hence, the uniform flow test cannot discriminate between the two formulations.

Mavriplis studied two time integrators BDF2 and ESDIRK64 [26]. To satisfy the DGCL for each integrator he requires that the uniform flow satisfy the discretized equations. He does this for a Finite Volume formulation of compressible flows, *i.e.* GCL compliance at levels 1 and 2. In the case of FVM, doing this defines a mesh velocity consistent with the space and time discretisation schemes.

Enforcing GCL compliance on the FEM conservative formulation (8) provides a rule for evaluating the divergence of the mesh velocity which will be denoted $(\nabla \cdot \mathbf{v}_d)$. However, it provides no rule on how to evaluate $\mathbf{v}_d$ itself, meaning that it does not define which mesh velocity $\mathbf{v}_d$ should be used in the ALE FEM. In this work, the rule for constructing the mesh velocity depends on whether the Butcher Tableau of the scheme is invertible or not.

6.1. GCL for time-stepping schemes with invertible Butcher tableaus

In this section, we consider time-stepping schemes for which Butcher tableaus are invertible. This embraces all Gauss, Radau and SDI Runge–Kutta schemes, i.e. IRK3 and 5 (see [43]). We also assume, as explained earlier in Section 2, that the mapping between $\Omega(0)$ and $\Omega(t)$ is given by a piecewise linear representation on the elements of the mesh. The Jacobian of this transformation is locally constant on each element of the mesh. Note however that J will be a function of time since the geometry of the element will change with time.

Proposition 2. *Consider a time-stepping scheme with an invertible Butcher tableau* $A = [a_{ij}]_{i,j\in[1,s]^2}$ *and let* $B = [b_{ij}]_{i,j\in[1,s]^2} = A^{-1}$ *be its inverse. Let* $J^{(t)}$ *be the determinant of the Jacobian transformation at time t from the reference domain* $\Omega(0)$ *to the deforming domain* $\Omega(t)$*. If we restrict ourselves to straight-sided triangular or tetrahedral elements, the following mesh velocity divergence formulation is a sufficient condition for compliance of the conservative formulation to levels 1 and 2 of the GCL (no-flow and uniform flow).*

$$\boxed{(\nabla \cdot v_d)^{(n+c_j)} = \sum_{k=1}^{s} b_{jk} \frac{J^{(n+c_k)} - J^{(n)}}{\Delta t J^{(n+c_j)}}, \quad j = 1,\ldots,s \qquad (18)}$$

Proof 2. The no-flow test is trivial since all terms in the conservative formulation are zero. Now, consider a uniform flow, the conservative formulation Eq. (8) over an element reduces to

$$\frac{d}{dt}\int_{\Omega_e(t)} \mathbf{w}\cdot\rho\mathbf{u}d\Omega = \int_{\Omega_e(t)} (\nabla\cdot\mathbf{v}_d)^{(t)}\mathbf{w}\cdot\rho\mathbf{u}d\Omega \tag{19}$$

Discretise this equation using Eq. (10) without the projection step (which is not required for time-stepping schemes with invertible Butcher tableaus) to obtain

$$\frac{1}{\Delta t}\int_{\Omega_e(n+c_i)} \mathbf{w}\cdot\rho\mathbf{u}d\Omega - \frac{1}{\Delta t}\int_{\Omega_e(n)} \mathbf{w}\cdot\rho\mathbf{u}d\Omega = \sum_{j=1}^{s} a_{ij}\int_{\Omega_e(n+c_j)} (\nabla\cdot\mathbf{v}_d)^{(n+c_j)}\mathbf{w}\cdot\rho\mathbf{u}d\Omega, \quad i = 1,\ldots,s \tag{20}$$

Now consider only the right-hand side (*RHS*) of Eq. (20). The essence of the proof consists in showing that the RHS of Eq. (20) is equal to the LHS. Insert the proposed expression of the mesh velocity divergence defined by Eq. (18). We have

$$RHS = \sum_{j=1}^{s} a_{ij}\int_{\Omega_e(n+c_j)} \sum_{k=1}^{s} b_{jk}\frac{J^{(n+c_k)} - J^{(n)}}{\Delta t J^{(n+c_j)}}\mathbf{w}\cdot\rho\mathbf{u}d\Omega, \quad i = 1,\ldots,s \tag{21}$$

For a linear representation of the geometry, *i.e.* straight-sided triangles or tetrahedra, $J^{(t)}$ is constant per element, so that $1/J^{(n+c_j)}$ is represented exactly by the spatial discretization scheme. In this case, Eq. (21) is numerically equivalent to

$$RHS = \sum_{j=1}^{s} a_{ij}\int_{\Omega_e(0)} \sum_{k=1}^{s} b_{jk}\frac{J^{(n+c_k)} - J^{(n)}}{\Delta t}\mathbf{w}\cdot\rho\mathbf{u}d\Omega, \quad i = 1,\ldots,s \tag{22}$$

For a constant uniform incompressible flow, $\rho\mathbf{u}$ does not depend on time. We also exploit the fact that on $\Omega(0)$, the test functions $\mathbf{w}(\mathbf{x})$ do not depend on time. We can now write

$$RHS = \sum_{j=1}^{s} a_{ij}\sum_{k=1}^{s} b_{jk}\int_{\Omega_e(0)} \frac{J^{(n+c_k)} - J^{(n)}}{\Delta t}\mathbf{w}\cdot\rho\mathbf{u}d\Omega, \quad i = 1,\ldots,s \tag{23}$$

Since B is the inverse of A, $a_{ij}b_{jk} = \delta_{ik},\ i,k = 1,\ldots,s$, with δ_{ik} the Kronecker symbol which is equal to one if $i = k$, and zero otherwise. The right-hand side reduces to

$$RHS = \int_{\Omega_e(0)} \frac{J^{(n+c_i)} - J^{(n)}}{\Delta t}\mathbf{w}\cdot\rho\mathbf{u}d\Omega, \quad i = 1,\ldots,s \tag{24}$$

and finally, since we restrict ourselves to a constant Jacobian per element, we get

$$RHS = \frac{1}{\Delta t}\int_{\Omega_e(n+c_i)} \mathbf{w}\cdot\rho\mathbf{u}d\Omega - \frac{1}{\Delta t}\int_{\Omega_e(n)} \mathbf{w}\cdot\rho\mathbf{u}d\Omega, \quad i = 1,\ldots,s \tag{25}$$

which completes the proof since we have equality with the left-hand side of Eq. (20). □

Remark: The proof has been performed over one element for simplicity and clarity. Summing over all elements of the mesh yields the result for the whole domain.

6.2. GCL for time-stepping schemes with non-invertible Butcher tableaus

For some popular time integrators, such as the Crank–Nicholson scheme, (a_{ij}) is not invertible. It is possible, however, to proceed in much the same way as in the previous section. We treat schemes which do not need a projection step. This means schemes for which the coefficients in Eq. (11) are equal to those of the last line of system (10), last row in the Butcher tableau. We exclude for brevity's sake Lobatto IIIB scheme, which would require consideration of the projection step in the discussion.

Proposition 3. *Consider a time-stepping scheme which does not require a projection step and for which the Butcher tableau* $A = [a_{ij}]_{i,j\in[s-p+1,s]\times[1,s]}$ *is not invertible but is of rank p equal to the number of implicit steps, from the* $s-p+1$th *to the* sth *step, the last p rows of A. Let* $J^{(t)}$ *be the determinant of the Jacobian transformation at time t from the reference domain* $\Omega(0)$ *to the deforming domain* $\Omega(t)$. *Then, if we restrict ourselves to straight-sided triangular or tetrahedral elements, there exists at least one vector* $[(\nabla\cdot\mathbf{v}_d)^{(n+c_j)}]_{j\in[1,s]}$ *such that*

$$\boxed{\frac{J^{(n+c_k)}-J^{(n)}}{\Delta t}=\sum_{j=1}^{s}a_{kj}J^{(n+c_j)}(\nabla\cdot\mathbf{v}_d)^{(n+c_j)},\quad k=s-p+1,\ldots,s \qquad (26)}$$

Then this constitutes a sufficient condition for compliance of the conservative formulation to levels 1 and 2 of the GCL (no-flow and uniform flow tests).

Proof 3. Consider a uniform flow, the conservative formulation equation (8) over an element reduces to

$$\frac{d}{dt}\int_{\Omega_e(t)}\mathbf{w}\cdot\rho\mathbf{u}d\Omega=\int_{\Omega_e(t)}(\nabla\cdot\mathbf{v}_d)(t)\mathbf{w}\cdot\rho\mathbf{u}\,d\Omega \qquad (27)$$

Discretising this equation using Eq. (10), yields

$$\frac{1}{\Delta t}\int_{\Omega_e(n+c_i)}\mathbf{w}\cdot\rho\mathbf{u}\,d\Omega-\frac{1}{\Delta t}\int_{\Omega_e(n)}\mathbf{w}\cdot\rho\mathbf{u}\,d\Omega=\sum_{j=1}^{s}a_{ij}\int_{\Omega_e(n+c_j)}(\nabla\cdot\mathbf{v}_d)^{(n+c_j)}\mathbf{w}\cdot\rho\mathbf{u}\,d\Omega,\quad i=s-p+1,\ldots,s \qquad (28)$$

which constitutes a system of p equations to be solved. For the class of Runge–Kutta schemes considered here, $A=[a_{ij}]_{i,j\in[s-p+1,s]\times[1,s]}$ is of rank p (see [43]). Hence there will be solution vectors $[(\nabla\cdot\mathbf{v})^{(n+c_j)}]_{j\in[1,s]}$ to system (28). □

For example, applying Eq. (26) to the Crank–Nicholson integrator and a uniform flow leads to the following equality (equivalent to GCL compliance at level 2) which must be satisfied

$$\frac{1}{2}J^{(n+1)}(\nabla\cdot\mathbf{v}_d)^{(n+1)}+\frac{1}{2}J^{(n)}(\nabla\cdot\mathbf{v}_d)^{(n)}=\frac{J^{(n+1)}-J^{(n)}}{\Delta t} \qquad (29)$$

As there are two unknowns ($(\nabla\cdot\mathbf{v}_d)$ at times n and $n+1$) several solution vectors $[(\nabla\cdot\mathbf{v}_d)^{(n+j)}]_{j\in[0,1]}$ are possible. We chose

$$(\nabla\cdot\mathbf{v}_d)^{(n)}=\frac{J^{(n+1)}-J^{(n)}}{\Delta tJ^{(n)}} \qquad (30)$$

$$(\nabla\cdot\mathbf{v}_d)^{(n+1)}=\frac{J^{(n+1)}-J^{(n)}}{\Delta tJ^{(n+1)}} \qquad (31)$$

Note that other choices are possible, for instance any convex combination of

$$(\tilde{\nabla}\cdot\mathbf{v}_d)^{(n)}=2a(\nabla\cdot\mathbf{v}_d)^{(n)} \qquad (32)$$

$$(\tilde{\nabla}\cdot\mathbf{v}_d)^{(n+1)}=2(1-a)(\nabla\cdot\mathbf{v}_d)^{(n+1)} \qquad (33)$$

$a\in\mathbb{R}$ will also work. This reflects the fact that there is more freedom in the choice of the mesh velocity divergence for time-stepping schemes with non-invertible Butcher tableaus.

At this point we have a general methodology, which accounts for characteristics of the time-stepping scheme, to construct the divergence of the mesh velocity to satisfy the GCL at level 2 (DGCL) on straight-sided triangles or tetrahedra. However, satisfying the DGCL does not automatically guarantee GCL compliance at level 3 as mentioned by Geuzaine et al. [25]. In fact, satisfying the DGCL does not provide any additional information about the convergence rate of the time-stepping procedure other than stating that the time-integrator will be at least first order accurate on deforming domains. While the technique for computing $(\nabla\cdot\mathbf{v}_d)$ is general, it provides no information about the proper way to compute $\mathbf{v}_d$ itself. This is the subject of the following section.

7. Mesh velocity calculation

The objective of this section is to define a mesh velocity such that accuracy observed on fixed grids is preserved on moving grids. Most previous works assume that the mesh velocity is given and is used to evaluate both $(\nabla\cdot\mathbf{v})$ and $\mathbf{v}$ in the conservative formulation (8). The only way to achieve GCL compliance is to find a time-integrator (or design one) such that it satisfies the GCL when the given mesh velocity is used for $\mathbf{v}$ and $(\nabla\cdot\mathbf{v})$ in Eq. (8).

We take a different approach and assume that the spatial discretisation and the time integrator are given, and we seek two formulas: one for evaluating the divergence of the mesh velocity $(\nabla\cdot\mathbf{v}_d)$ to satisfy the GCL, and a second one to compute the mesh velocity itself $\mathbf{v}_m$ so as to ensure that the high order temporal accuracy observed on a fixed mesh is maintained on a deforming mesh. This amounts to using two mesh velocities $\mathbf{v}_d$ and $\mathbf{v}_m$. As shown in Section 6, only $(\nabla\cdot\mathbf{v}_d)$ is required to evaluate the term $\int_{\Omega(t)}\mathbf{w}\cdot(\nabla\cdot\mathbf{v}_d)\rho\mathbf{u}d\Omega$ and provide GCL compliance at level 2 for Eq. (8). The velocity $\mathbf{v}_d$ itself is not required. The second mesh velocity $\mathbf{v}_m$ appears only in $\int_{\Omega(t)} \mathbf{w} \cdot \rho[(\mathbf{u} - \mathbf{v}_m) \cdot \nabla]\mathbf{u} d\Omega$. Hence, $(\nabla \cdot \mathbf{v}_m)$ need not be GCL compliant. Its role is to ensure that the fixed mesh temporal accuracy of the time integrator is also observed on deforming meshes.

In this approach it is clear that GCL compliance has no effect on the temporal accuracy of the time integrator. In fact, the freedom resulting from the use of two mesh velocities provides the mechanism to maintain the fixed grid temporal accuracy when the scheme applied to deforming domains. This approach offers several advantages. The same time integrator is used for fixed mesh and deforming meshes. This greatly simplifies code structure, software maintenance and modifications, use of the code, and interpretation of results. We now take a look at possible constructions of $\mathbf{v}_m$ for the three time-integrators of the previous sections. Here too the construction of $\mathbf{v}_m$ is different depending on whether the Crank–Nicholson or IRK3 and IRK5 schemes are used just as was the case for $(\nabla \cdot \mathbf{v}_d)$.

7.1. The Crank–Nicholson scheme

We begin by taking a look at this issue for the Crank–Nicholson scheme for which the usual and accepted way of evaluating the mesh velocity is the midpoint rule

$$\boxed{\mathbf{v}_m(\mathbf{x}) = \frac{\mathbf{x}^{(n+1)} - \mathbf{x}^{(n)}}{\Delta t}} \tag{34}$$

This formula is used to compute the mesh velocity $\mathbf{v}_m$. However, its use to evaluate the mesh velocity divergence is restricted to 2D problems as stated by the following proposition. It cannot be used in 3D.

Proposition 4. *Consider the conservative formulation equation (8) and piecewise linear mesh deformation in space (linear deformation of triangles or tetrahedra). Using the divergence of Eq. (34) to evaluate the divergence of the mesh velocity, $(\nabla \cdot \mathbf{v}_d) = (\nabla \cdot \mathbf{v}_m)$, will result in GCL compliance at levels 1 and 2 for 2D flows only.*

Proof 4. We substitute Eq. (34) into the GCL equation (29). We restrict the proof over one element for clarity of the notation. Let Ω_e be a two-dimensional elementary domain

$$\begin{aligned}\frac{1}{\Delta t}\int_{\Omega_e(n+1)} \mathbf{w} \cdot \rho \mathbf{u} \, d\Omega - \frac{1}{\Delta t}\int_{\Omega_e(n)} \mathbf{w} \cdot \rho \mathbf{u} \, d\Omega = {} & \frac{1}{2}\int_{\Omega_e(n)} \left(\nabla^{(n)} \cdot \frac{\mathbf{x}^{(n+1)} - \mathbf{x}^{(n)}}{\Delta t}\right)\mathbf{w} \cdot \rho \mathbf{u} \, d\Omega \\ & + \frac{1}{2}\int_{\Omega_e(n+1)} \left(\nabla^{(n+1)} \cdot \frac{\mathbf{x}^{(n+1)} - \mathbf{x}^{(n)}}{\Delta t}\right)\mathbf{w} \cdot \rho \mathbf{u} \, d\Omega\end{aligned} \tag{35}$$

For this equation, $\nabla^{(n+1)} \cdot \mathbf{x}^{(n+1)} = 2$ and $\nabla^{(n)} \cdot \mathbf{x}^{(n)} = 2$ in two-dimensions only. Thus to satisfy Eq. (35) the following relationship must hold

$$\int_{\Omega_e(n+1)} (\nabla^{(n+1)} \cdot \mathbf{x}^{(n)})\mathbf{w} \cdot \rho \mathbf{u} \, d\Omega = \int_{\Omega_e(n)} (\nabla^{(n)} \cdot \mathbf{x}^{(n+1)})\mathbf{w} \cdot \rho \mathbf{u} \, d\Omega \tag{36}$$

Now consider the transformation $\mathbf{T}^{(n)}(r,s)$ and $\mathbf{T}^{(n+1)}(r,s)$ from the reference element $\Omega_e(0)$ to the physical element $\Omega_e(t)$ at times n and $n+1$.

$$\begin{aligned}&\mathbf{T}^{(n)} : (r,s) \mapsto (x^{(n)}, y^{(n)}) \\ &\mathbf{T}^{(n+1)} : (r,s) \mapsto (x^{(n+1)}, y^{(n+1)})\end{aligned}$$

and let $\mathbf{F}$ be the Jacobian of the transformations from the reference element to the physical element and J its determinant. We have

$$\mathbf{F}^{(n)} = \begin{bmatrix} \frac{\partial x^{(n)}}{\partial r} & \frac{\partial x^{(n)}}{\partial s} \\ \frac{\partial y^{(n)}}{\partial r} & \frac{\partial y^{(n)}}{\partial s} \end{bmatrix}, \quad \mathbf{F}^{(n+1)} = \begin{bmatrix} \frac{\partial x^{(n+1)}}{\partial r} & \frac{\partial x^{(n+1)}}{\partial s} \\ \frac{\partial y^{(n+1)}}{\partial r} & \frac{\partial y^{(n+1)}}{\partial s} \end{bmatrix}$$

Then Eq. (36) becomes

$$\int_{\Omega_e(0)} J^{(n+1)}\nabla \cdot (\mathbf{F}^{(n+1)^{-1}}\mathbf{F}^{(n)}\mathbf{x})\mathbf{w} \cdot \rho \mathbf{u} \, d\Omega \tag{37}$$

$$= \int_{\Omega_e(0)} J^{(n)}\nabla \cdot (\mathbf{F}^{(n)^{-1}}\mathbf{F}^{(n+1)}\mathbf{x})\mathbf{w} \cdot \rho \mathbf{u} \, d\Omega \tag{38}$$

Recall that for straight-sided triangular or tetrahedral elements, J and $\mathbf{F}$ are piecewise constant, so that

$$\nabla \cdot (\mathbf{F}^{(n+1)^{-1}}\mathbf{F}^{(n)}\mathbf{x}) = \mathrm{tr}[\mathbf{F}^{(n+1)^{-1}}\mathbf{F}^{(n)}] \tag{39}$$

$$\nabla \cdot (J^{(n)}/J^{(n+1)}\mathbf{F}^{(n)^{-1}}\mathbf{F}^{(n+1)}\mathbf{x}) = \mathrm{tr}\{\mathrm{Cof}[\mathbf{F}^{(n+1)^{-1}}\mathbf{F}^{(n)}]\} \tag{40}$$

Satisfying the equality implies that the following expression must be verified

$$\mathrm{tr}[\mathbf{F}^{(n+1)^{-1}}\mathbf{F}^{(n)}] = \mathrm{tr}\{\mathrm{Cof}[\mathbf{F}^{(n+1)^{-1}}\mathbf{F}^{(n)}]\} \tag{41}$$

Setting $\mathbf{A} = \mathbf{F}^{(n+1)^{-1}}\mathbf{F}^{(n)}$ in Eq. (41) is equivalent to having $\mathrm{tr}(\mathbf{A}) = \mathrm{tr}[\mathrm{Cof}(\mathbf{A})]$. This equality holds for matrices of rank 2 only. This means that taking the divergence of formula (34) will yield a GCL compliant mesh velocity divergence for two-dimensional problems only. In 3D $\nabla^{(n+1)} \cdot \mathbf{x}^{(n+1)} = \nabla^{(n)} \cdot \mathbf{x}^{(n)} = 3$. One could think to multiply the mesh velocity by 2/3. However, Eq. (41) will generally not be satisfied in 3D. □

Remark: It is preferable to use Eqs. (30) and (31) to evaluate $(\nabla \cdot \mathbf{v}_d)$ as they guarantee GCL compliance at level 2 in both two and three dimensions.**Remark**: Lesoinne and Farhat [4] successfully used formula (34) for 2D flows only. For 3D flows they replaced the CN scheme by a more costly multipoint time integrator to achieve GCL compliance. In our approach, the distinction we make between the mesh velocity divergence $(\nabla \cdot \mathbf{v}_d)$ and the mesh velocity $(\mathbf{v}_m)$, results in time discretisations that are 2D and 3D GCL compliant. This allows us to use the same identical formulation for 2D or 3D flow simulations.

7.2. IRK Radau schemes (invertible Butcher tableaus)

Generalizing Eq. (34) to IRK3 and IRK5 time-stepping schemes yields

$$\boxed{\mathbf{v}_m^{(n+c_j)}(\mathbf{x}) = \sum_{i=1}^{s}[a_{ij}]^{-1}\frac{\mathbf{x}^{(n+c_i)} - \mathbf{x}^{(n)}}{\Delta t}} \tag{42}$$

This formula may be used to compute the mesh velocity $\mathbf{v}_m$. However, its use to evaluate the mesh velocity divergence is restricted to 2D problems and mesh motions that are linear functions of time, a severe restriction, as stated by the following proposition.

Proposition 5. *Consider the conservative formulation equation (8) and piecewise linear deformations in space (straight-sided triangles or tetrahedra). Using divergence of Eq. (42) to evaluate the divergence of the mesh velocity, $(\nabla \cdot \mathbf{v}_d) = (\nabla \cdot \mathbf{v}_m)$, will make the conservative formulation satisfy the GCL only if the mesh motion is a linear function of time and only for 2D flows.*

Proof 5. The proof is given for the IRK3 scheme. A similar argument applies to the IRK5 scheme. We restrict the proof over one element for clarity of the notation. Let Ω_e be a two-dimensional elementary domain. Consider the second step of the IRK3 integrator, Eq. (14). Substituting the conservative formulation Eq. (8) and the divergence of Eq. (42) for evaluating the mesh velocity divergence for a uniform flow yields

$$\begin{aligned}\frac{1}{\Delta t}\int_{\Omega_e(n+1)} \mathbf{w}\cdot\rho\mathbf{u}d\Omega - \frac{1}{\Delta t}\int_{\Omega_e(n)} \mathbf{w}\cdot\rho\mathbf{u}\,d\Omega &= \frac{3}{4}\int_{\Omega_e(n+1/3)}\left[\nabla^{(n+1/3)}\cdot\left(\frac{3}{2}\frac{\mathbf{x}^{(n+1/3)}-\mathbf{x}^{(n)}}{\Delta t} + \frac{1}{2}\frac{\mathbf{x}^{(n+1)}-\mathbf{x}^{(n)}}{\Delta t}\right)\right]\mathbf{w}\cdot\rho\mathbf{u}\,d\Omega \\ &\quad + \frac{1}{4}\int_{\Omega_e(n+1)}\left[\nabla^{(n+1)}\cdot\left(-\frac{9}{2}\frac{\mathbf{x}^{(n+1/3)}-\mathbf{x}^{(n)}}{\Delta t} + \frac{5}{2}\frac{\mathbf{x}^{(n+1)}-\mathbf{x}^{(n)}}{\Delta t}\right)\right]\mathbf{w}\cdot\rho\mathbf{u}\,d\Omega\end{aligned} \tag{43}$$

Now letting the mesh motion be a linear function of time leads to the following property

$$\mathbf{x}^{(n+1/3)} - \mathbf{x}^{(n)} = \frac{\mathbf{x}^{(n+1)} - \mathbf{x}^{(n)}}{3} \tag{44}$$

Substitution of Eq. (44) into the right-hand side of Eq. (43) leads to

$$\mathrm{RHS} = \frac{3}{4}\int_{\Omega_e(n+1/3)}\left[\nabla^{(n+1/3)}\cdot\left(\frac{\mathbf{x}^{(n+1)}-\mathbf{x}^{(n)}}{\Delta t}\right)\right]\mathbf{w}\cdot\rho\mathbf{u}\,d\Omega + \frac{1}{4}\int_{\Omega_e(n+1)}\left[\nabla^{(n+1)}\cdot\left(\frac{\mathbf{x}^{(n+1)}-\mathbf{x}^{(n)}}{\Delta t}\right)\right]\mathbf{w}\cdot\rho\mathbf{u}\,d\Omega \tag{45}$$

Transform the first term of the right-hand side above using Eq. (36) which holds for two-dimensional flows only

$$\begin{aligned}\mathrm{RHS} &= \frac{3}{4}\int_{\Omega_e(n+1)}\left[\nabla^{(n+1)}\cdot\left(\frac{\mathbf{x}^{(n+1/3)}}{\Delta t}\right)\right]\mathbf{w}\cdot\rho\mathbf{u}\,d\Omega - \frac{3}{4}\int_{\Omega_e(n)}\left[\nabla^{(n)}\cdot\left(\frac{\mathbf{x}^{(n+1/3)}}{\Delta t}\right)\right]\mathbf{w}\cdot\rho\mathbf{u}\,d\Omega \\ &\quad + \frac{1}{4}\int_{\Omega_e(n+1)}\left[\nabla^{(n+1)}\cdot\left(\frac{\mathbf{x}^{(n+1)}-\mathbf{x}^{(n)}}{\Delta t}\right)\right]\mathbf{w}\cdot\rho\mathbf{u}\,d\Omega\end{aligned} \tag{46}$$

Use property Eq. (44) to obtain

$$\begin{aligned}\mathrm{RHS} &= \frac{3}{4}\int_{\Omega_e(n+1)}\left[\nabla^{(n+1)}\cdot\left(\frac{\mathbf{x}^{(n+1)}+2\mathbf{x}^{(n)}}{3\Delta t}\right)\right]\mathbf{w}\cdot\rho\mathbf{u}\,d\Omega - \frac{3}{4}\int_{\Omega_e(n)}\left[\nabla^{(n)}\cdot\left(\frac{\mathbf{x}^{(n+1)}+2\mathbf{x}^{(n)}}{3\Delta t}\right)\right]\mathbf{w}\cdot\rho\mathbf{u}\,d\Omega \\ &\quad + \frac{1}{4}\int_{\Omega_e(n+1)}\left[\nabla^{(n+1)}\cdot\left(\frac{\mathbf{x}^{(n+1)}-\mathbf{x}^{(n)}}{\Delta t}\right)\right]\mathbf{w}\cdot\rho\mathbf{u}\,d\Omega\end{aligned} \tag{47}$$

Finally, using Eq. (36) once more leads to

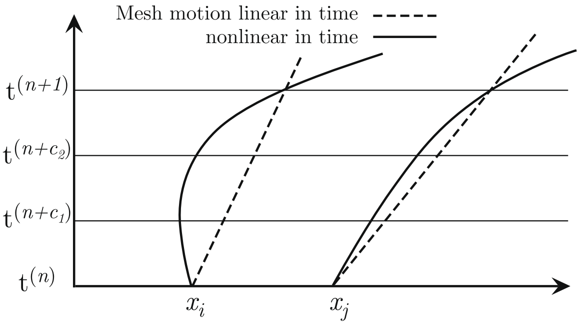

Fig. 1. Examples of linear and nonlinear mesh motions within a time step $[t^{(n)}, t^{(n+1)}]$.

$$\mathrm{RHS} = \frac{1}{2}\int_{\Omega_e(n+1)}\left[\nabla^{(n+1)}\cdot\left(\frac{\mathbf{x}^{(n+1)}}{\Delta t}\right)\right]\mathbf{w}\cdot\rho\mathbf{u}\,d\Omega - \frac{1}{2}\int_{\Omega_e(n)}\left[\nabla^{(n)}\cdot\left(\frac{\mathbf{x}^{(n)}}{\Delta t}\right)\right]\mathbf{w}\cdot\rho\mathbf{u}\,d\Omega \tag{48}$$

In two dimensions, we have $\nabla^{(n)}\cdot\mathbf{x}^{(n)} = \nabla^{(n+1)}\cdot\mathbf{x}^{(n+1)} = 2$. Thus, Eq. (48) equals the left-hand side of (43). However, the use of Eq. (36) is restricted to 2D and Eq. (44) to a linear time dependence of the mesh motion so that Eqs. (43) is subjected to both restrictions. □

Remark: It is preferable to use Eq. (18) to evaluate $(\nabla\cdot\mathbf{v}_d)$ as it allows for GCL compliance at level 2 in both two and three dimensions and mesh motions that are arbitrary functions of time.

Remark: For practical cases the mesh motion is arbitrary so that it is not a linear function of time. Hence the mesh velocity defined by Eq. (42) will not be GCL compliant for multi-step schemes, such as IRK3 and IRK5 schemes. Fig. 1 illustrates mesh motions that are linear and non-linear functions of time. Taking the divergence of Eq. (42) will not yield the result of Eq. (18). Thus, Eq. (42) cannot lead to GCL compliance in the general case.

The only remaining question is whether the convergence rate of the time stepping scheme is optimal (GCL at level 3), *i.e.* do we have the same convergence rate on moving meshes as on fixed meshes. This will be answered in Section 8 where we perform numerical tests on the IRK3 and IRK5 time integrators using nonlinear mesh motions.

We briefly summarize our results thus far. The conservative weak form from Eq. (8) will be GCL compliant if

(1) the mesh consists of linearly deforming straight-sided triangles in 2D or tetrahedra in 3D,
(2) the following definitions are used for $(\nabla\cdot\mathbf{v}_d)$ and $\mathbf{v}_m$ for IRK3 and IRK5

$$(\nabla\cdot\mathbf{v}_d)^{(n+c_j)} = \sum_{i=1}^{s}[a_{ij}]^{-1}\frac{J^{(n+c_i)} - J^{(n)}}{\Delta t J^{(n+c_j)}}, \quad j = 1,\ldots,s \tag{49}$$

$$\mathbf{v}_m^{(n+c_j)}(\mathbf{x}) = \sum_{i=1}^{s}[a_{ij}]^{-1}\frac{\mathbf{x}^{(n+c_i)} - \mathbf{x}^{(n)}}{\Delta t}, \quad j = 1\ldots s \tag{50}$$

or the following definitions for $(\nabla\cdot\mathbf{v}_d)$ and $\mathbf{v}_m$ for the Crank–Nicholson scheme

$$(\nabla\cdot\mathbf{v}_d)^{(n+j)} = \frac{J^{(n+1)} - J^{(n)}}{\Delta t J^{(n+j)}}, \quad j = 0,1 \tag{51}$$

$$\mathbf{v}_m^{(n+j)}(\mathbf{x}) = \frac{\mathbf{x}^{(n+1)} - \mathbf{x}^{(n)}}{\Delta t}, \quad j = 0,1 \tag{52}$$

Furthermore, the time integrators will exhibit optimal temporal accuracy that is the fixed mesh temporal convergence rate will be observed on deforming meshes.

8. Analytical and numerical results

This section presents results from analytical error analysis and careful numerical tests verifying that our approach yields optimal temporal accuracy for the CN, IRK3 and IRK5 integrators. This is achieved by considering two separate classes of unsteady solutions. The first regroups solutions that are represented exactly by the spatial discretisation: the uniform, Couette and Poiseuille flows. For these flows, there are no interaction or interference between the temporal and spatial discretisation errors so that accuracy of the time-stepping scheme can be tested without worrying about spatial discretisation artifacts.

The second kind of unsteady solutions is a manufactured solution of a very general nature that cannot be represented exactly by the finite element basis functions. We use the Method of Manufactured Solution (MMS) [44] to construct a solution of sufficient complexity on a deforming domain to ensure that all terms in the ALE formulation are exercised. This analytical Manufactured Solution makes it possible to perform time step refinement studies to draw definite conclusions about time accuracy.

8.1. Uniform flow test

The uniform flow test $\mathbf{u} = 1$ is not a very discriminating test for the non-conservative formulation equation (7) as shown by Formaggia et al. [17]. Since the fluid velocity is constant, its derivatives vanish, so that the mesh velocity term $\int \mathbf{w} \cdot \rho[(\mathbf{u} - \mathbf{v}_m) \cdot \nabla]\mathbf{u}$ is identically 0 and has no effects whatsoever on the result. For the conservative formulation, use of Eq. (49) and (51) (see Section 6) is required to satisfy GCL at level 2, depending on the time-stepping scheme.

For the uniform flow test, Eq. (7) or Eq. (8) result in simple algebraic equations that can be evaluated and analyzed easily. Our numerical results confirmed that no parasitic flow solution arises with either formulations, and velocities as well as pressure maintain machine accuracy for all times. In other words, both formulations satisfy the so-called uniform flow test (GCL compliance at levels 1 and 2). However, it provides no means for testing GCL compliance at level 3 as levels 1 and 2 are insufficient to discriminate. Doing this requires a slightly more involved flow field as shown in the next sections.

8.2. The linear shear flow

The linear shear flow or Couette flow is usually associated with the flow between two flat plates with one moving in its plane relative to the other. Driven by viscosity, the flow is a linear function of y (see [29])

$$u = y \tag{53}$$

$$v = 0 \tag{54}$$

$$p = \text{constant} \tag{55}$$

Even though the flow is steady one can still analyse the GCL provided the grid points inside the domain move so that the mesh deforms with time. This test exercises both the GCL and the mesh velocity $\int_{\Omega(t)} \mathbf{w} \cdot \rho[(\mathbf{u} - \mathbf{v}_m) \cdot \nabla]\mathbf{u} \neq 0$. This problem is useful because it lends itself to a complete analytical analysis of the time truncation error. Since $\mathbf{u}$ is linear in y and p is constant, the spatial variations of the flow are represented exactly by the FE discretisation. Hence the only contribution to the error is the temporal discretisation.

This simplified setting is ideal to carry out a detailed time truncation error analysis of the conservative formulation, Eq. (8), with the Crank–Nicholson time integrator on arbitrary but spatially linear mesh motions. Recall that the popular CN scheme is also a Runge–Kutta so that its time truncation error is given by [45]

$$\epsilon^{(n+c_i)}(\Delta t) = \frac{y^{(n+c_i)} - y^{(n)}}{\Delta t} - \sum_{j=1}^{s} a_{ij}\phi(t^{(n+c_j)}, y^{(n+c_j)}), \quad \text{for } i = 1, \ldots, s \tag{56}$$

Proposition 6. *If the conservative formulation equation (8) is used in conjunction with Eqs. (51) and (52), for spatially linear deformation of triangles or tetrahedra, the Crank–Nicholson scheme will yield the exact solution to the linear shear flow on deforming grids.*

Proof 6. Consider time integration over one time-step from $t^{(n)}$ to $t^{(n+1)} = t^{(n)} + \Delta t$ for linearly deforming triangles (2D) or tetrahedra (3D)

$$\begin{aligned}\epsilon_{CN}^{(n+1)}(\Delta t) = {} & \frac{1}{\Delta t}\int_{\Omega_e(n+1)} \mathbf{w} y \, d\Omega - \frac{1}{\Delta t}\int_{\Omega_e(n)} \mathbf{w} y \, d\Omega - \frac{1}{2}\int_{\Omega_e(n+1)} \mathbf{w}(\nabla \cdot \mathbf{v}_d)^{(n+1)} y \, d\Omega \\ & - \frac{1}{2}\int_{\Omega_e(n)} \mathbf{w}(\nabla \cdot \mathbf{v}_d)^{(n)} y \, d\Omega - \frac{1}{2}\int_{\Omega_e(n+1)} \mathbf{w} v_m^{(n+1)} \, d\Omega - \frac{1}{2}\int_{\Omega_e(n)} \mathbf{w} v_m^{(n)} \, d\Omega\end{aligned} \tag{57}$$

Due to the linear representation of the geometry, substitution of expressions for the mesh velocity divergence eqquation (51) and mesh velocity equation (52) into Eq. (57) yields

$$\begin{aligned}\epsilon_{CN}^{(n+1)}(\Delta t) = {} & \int_{\Omega_e(n)} \mathbf{w}\left\{\frac{J^{(n+1)}(y + v_m\Delta t) - y}{J^{(n)}\Delta t}\right\} d\Omega - \frac{1}{2}\int_{\Omega_e(n)} \mathbf{w}\left\{\frac{J^{(n+1)} - 1}{J^{(n)}\Delta t}[(y + v_m\Delta t) + y]\right\} d\Omega \\ & - \frac{1}{2}\int_{\Omega_e(n)} \mathbf{w}\left\{v_m\left(\frac{J^{(n+1)}}{J^{(n)}} + 1\right)\right\} d\Omega\end{aligned} \tag{58}$$

Note that with our definition of the mesh velocity $\mathbf{v}_m$, transforming integral over $\Omega(n+1)$ to integral over $\Omega(n)$ also transforms naturally y to $y + v_m\Delta t$ which is advantageous from an analytical standpoint. Since, v_m is spatially linear, it is easily shown that $\epsilon_{CN}(\Delta t) = 0$ will be satisfied to machine zero. □

Remark: This behaviour is exceptional, and occurs only with this test case. This performance is superior to that of Lesoinne and Farhat [4].

Remark: Applying the same procedure to the non-conservative formulation we find that the error is $\int_{\Omega_e(n)} \mathbf{w}\cdot v_m(J^{(n+1)}-J^{(n)})/J^{(n)}\,d\Omega$ so that the time truncation error comes out to be of order one, $\mathcal{O}(\Delta t)$. This implies that, at best, only first order time accuracy can be achieved with the non-conservative formulation equation (7) if formula (52) is used.

Remark: The method developed by Lesoinne and Farhat [4] with respect to the Crank–Nicholson will reproduce the exact solution with 2nd order time accuracy less than above. This is due to the fact that they compute directly the mesh velocity divergence from the mesh velocity instead of using Eq. (51). This is an example of proposition 3 which states that more than one mesh velocity divergence may yield GCL compliance for the Crank–Nicholson scheme. Lesoinne's results and ours are two examples yielding GCL compliance at level 3. However, Lesoinne's yields optimal time accuracy for 2D flows only as seen previously while the present method is valid for 2D and 3D.

Proposition 7. *If the conservative formulation equation (8) is used in conjunction with Eqs. (49) and (50), for linear deformations of triangles or tetrahedra and if the mesh motion is a linear function of time, IRK3 and IRK5 schemes will yield the exact solution to the linear shear flow on deforming grids.*

Proof 7. We give the proof for the IRK3 scheme. A similar argument applies to the IRK5 integrator. Consider the time truncation error (56) for Radau IIa3 scheme (IRK3). The second substep applied to the linear shear flow reads

$$\begin{aligned}\epsilon_{IRK3}^{(n+1)}(\Delta t) = {} & \frac{1}{\Delta t}\int_{\Omega_e(n+1)} \mathbf{w} y\, d\Omega - \frac{1}{\Delta t}\int_{\Omega_e(n)} \mathbf{w} y\, d\Omega + \frac{3}{4}\int_{\Omega_e(n+1/3)} \mathbf{w}[(\nabla\cdot\mathbf{v}_d)^{(n+1/3)} y - v_m^{(n+1/3)}]d\Omega \\ & + \frac{1}{4}\int_{\Omega_e(n+1)} \mathbf{w}[(\nabla\cdot\mathbf{v}_d)^{(n+1)} y - v_m^{(n+1)}]d\Omega \end{aligned} \tag{59}$$

The mesh motion is linear in space and time. Using formula (49) in Eq. (59) leads to $\epsilon_{IRK3}^{(n+1)}(\Delta t) = 0$. □

To reinforce the above conclusions, we complete this analytical study with a numerical time step refinement study. The solution is advanced in time on the time interval [0,4] starting with one time step Δt that we repeatedly divide by 2. Thus

$$\Delta t_k = 4/2^{k-1}, \quad k \in [1,7] \tag{60}$$

The errors for the velocity and pressure fields are evaluated at time $t = 4$ using the following error norms

$$||e_u||_E^2 = ||u_{ex} - u_h||_E^2 = \int_\Omega (\tau_{ex} - \tau_h) : (\tau_{ex} - \tau_h) d\Omega \tag{61}$$

for the velocity and

$$||e_p||_{L_2}^2 = ||p_{ex} - p_h||_{L_2}^2 = \int_\Omega (p_{ex} - p_h)^2 d\Omega \tag{62}$$

for the pressure. Subscript *ex* refers to the exact solution and *h* to the finite element solution.

Fig. 2 presents results obtained for the Couette Flow using the following mesh motion:

$$\text{horizontal} \quad \xi(x,y,t) = t(1-x^2)(y+1)/32 \tag{63}$$

$$\text{vertical} \quad \eta(x,y,t) = t(1-y^2)(x+t(1-x^2)/32+1)/32 \tag{64}$$

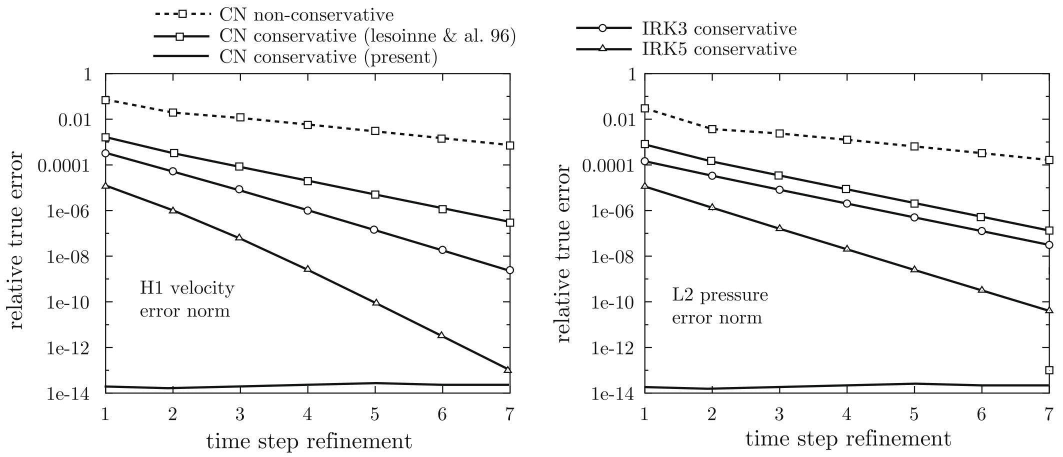

Fig. 2. Grid convergence study for the Couette flow with mesh moving in the two directions.

It exhibits a nonlinear (quadratic) dependence in t so that this test will be sensitive to choices made for evaluating $(\nabla \cdot \mathbf{v}_d)$ and $\mathbf{v}_m$. In particular, $(\nabla \cdot \mathbf{v}_d) \neq (\nabla \cdot \mathbf{v}_m)$ for IRK3 and IRK5 schemes. As we can observe in Fig. 2, the non-conservative CN algorithm presents a suboptimal convergence rate of $\mathcal{O}(\Delta t)$ as predicted by the analytical study. Note also that the convergence rates for the other schemes are optimal; that is they are equal to those observed on fixed meshes. These results confirm our analytical error analysis. The non-conservative formulation exhibits a suboptimal convergence rate of one for all time integrators whereas the conservative formulation exhibits the time integrator's optimal rate.

Our Crank–Nicholson yields the exact solution because the mesh velocity and the divergence of the mesh velocity are evaluated with Eqs. (51) and (52). This unusual behavior results from a special property of our approach. For the ODE $y' = f(t, y)$ it is written as

$$\frac{y^{(n+1)} - y^{(n)}}{\Delta t} = \frac{f(t^{(n)}, y^{(n)}) + f(t^{(n+1)}, y^{(n+1)})}{2} \tag{65}$$

Because this Crank–Nicholson scheme does not sample the solution at intermediate time steps, it always perceives the mesh motion as a linear function of time which explains why our CN conservative formulation delivers the exact solution as predicted by proposition 6.

To verify our statement that multi-step methods yield the exact solution to the Couette flow when the mesh motion is a linear function of time, we ran the three schemes with the conservative formulation. All integrators reproduced the exact solution to the Couette flow with velocity and pressure errors of order of machine zero ($\approx 10^{-14}$) as predicted by proposition 7.

Table 2 summarizes results for the Couette flow, the different formulations and time integrators with the proposed combination of mesh velocity and mesh velocity divergence. The non-conservative formulation yields a solution that is first order accurate, $\mathcal{O}(\Delta t)$, for the three time integrators. The conservative formulation yields solutions with optimal time accuracy. Thus, there appears to be compelling evidence for using the conservative formulation, Eq. (8).

We note, however, that the Couette flow does not thoroughly test the viscous terms in the Navier–Stokes equations as the second derivatives of velocity and the convective terms vanish for this flow.

Remark: While the above error analyses (prop 6 and 7) hold formally for both 2D and 3D simplices, optimal accuracy remains to be confirmed by numerical tests in 3D for all test cases presented in the following section, including 3D manufactured solution.

The following sections present systematic and thorough numerical tests confirming the theoretical results for two-dimensional flows.

8.3. The Poiseuille flow

The Poiseuille flow (see [29]) provides a test for some of the viscous terms in the Navier–Stokes equations. The velocity component u is a quadratic polynomial in y only, v is zero, and p is linear in x only. The solution is again steady state and

Table 2
Convergence rate for various time-stepping schemes for the Couette flow and linear/nonlinear time mesh motions.

	Conservative formulation (8)		Non-conservative formulation (7)	
	L_2-pressure	H^1-energy	L_2-pressure	H^1-energy
Nonlinear $\mathbf{v}_m$				
Crank–Nicholson	Exact	Exact	1	1
IRK3	2	3	1	1
IRK5	3	5	1	1
Linear $\mathbf{v}_m$				
Crank–Nicholson	Exact	Exact	1	1
IRK3	Exact	Exact	1	1
IRK5	Exact	Exact	1	1

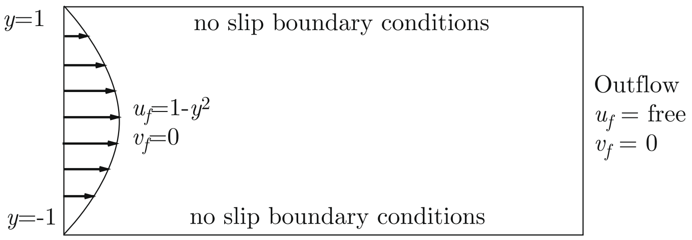

Fig. 3. Geometry and boundary conditions for the Poiseuille flow.

independent of t as for the Couette and uniform flows. The problem is made unsteady by using a time varying mesh. We use the same mesh motion as for the Couette flow equations (63) and (64).

The time integration is performed on the time interval $[0,1]$ with the following sequence of time steps

$$\Delta t_k = 1/2^{k-1}, \quad k \in [1,7] \tag{66}$$

Geometry and boundary conditions are depicted in Fig. 3. Again only vertices inside the domain are allowed to move.

Fig. 4 and Table 3

Remark: We performed an analytical study similar to that done for the linear shear flow and the CN scheme. For the conservative formulation and Eqs. (52) and (51), it shows that the time truncation error term is

$$\int_{\Omega(n)} \mathbf{w}(-v_m^2/2)\Delta t(J^{(n+1)} - J^{(n)})/J^{(n)}\, d\Omega$$

which is of order of $\mathcal{O}(\Delta t^2)$ and confirms the numerical results. Moreover, this analysis shows that the results are independent of space dimension for linear deforming triangles or tetrahedra.

We note that the Poiseuille flow is not a truly conclusive test for an ALE formulation because the solution is one-dimensional, the convective terms are zero, and the solution is represented exactly by the finite element space discretisation. A test case with a more complex flow pattern given by the Method of Manufactured Solutions is required.

8.4. Manufactured Solution

The Method of Manufactured Solutions provides a more exhaustive and general test of the two formulations. In fact the Method of Manufactured Solutions [44] provides for a complete verification of the time-integrators-GCL formulations. Manufactured solutions are constructed in such a way that they exercise all derivatives in the flow equations. The manufactured velocity and pressure solutions are set to

$$\begin{aligned}
u(x,y,t) &= (-1 + x + x^2 + y + y^2 + xy + y^3)g(t)\\
v(x,y,t) &= (1 + x + x^2 - y - y^2/2 - 2xy + x^3)g(t)\\
p(x,y,t) &= x^2\\
g(t) &= 1 + \tanh(t)\sin(9\pi t)\\
\xi(x,y,t) &= xyt^2/5\\
\eta(x,y,t) &= xy(1 - t^2/5)/10
\end{aligned}$$

This solution is not represented exactly by the spatial discretisation of the P2–P1 Taylor–Hood element used here so that the spatial discretisation contributes to the overall error. The FE approximation is second order accurate for velocity in H^1 norm (3rd order in L_2 norm) and second order accurate for the pressure in L_2 norm.

Initial tests with the manufactured solution were disappointing. Because with IRK3 and IRK5 schemes, the time truncation error decreases extremely fast with Δt so that after 1–3 steps of refinement the spatial discretisation error dominates the total error. Hence the convergence curves will reach plateaus. Reducing the level of this plateau requires such fine meshes that the computations are impractical to perform. The iterated Richardson extrapolation method provides a very effective alternative to the usual approach described by Roache [44] (see Appendix A). It provides a reference solution which corresponds to the exact solution to the system of ordinary differential equations in time resulting from the Finite Element discretisation of space.

The initial conditions are given by evaluating the manufactured solution at $t = 0$. Simulations are performed over the time interval [0, 0.5] with

$$\Delta t_k = 1/2^k, \quad k \in [1, 12] \tag{67}$$

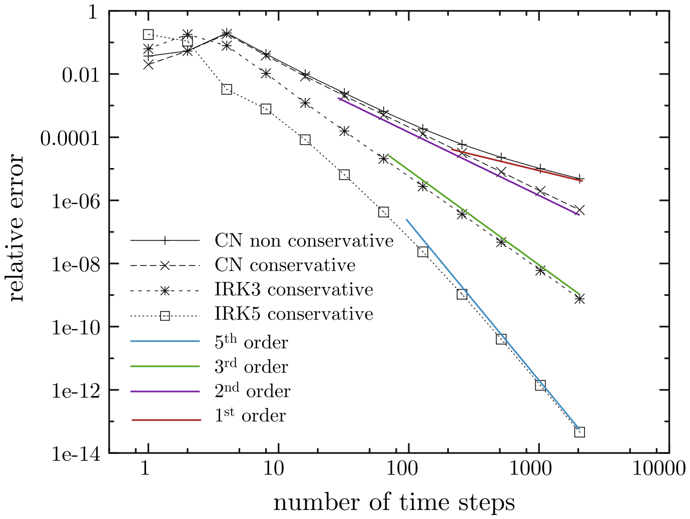

Fig. 6. Grid convergence for the manufactured solution, H^1 energy norm.

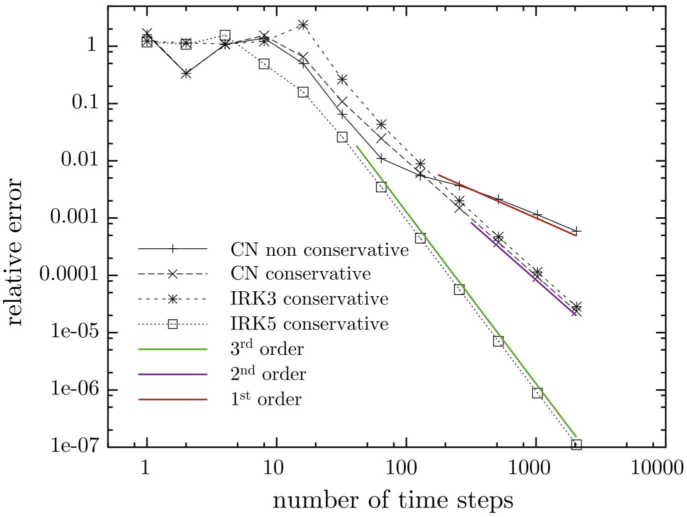

Fig. 7. Grid convergence for the manufactured solution, L_2 pressure norm.

Table 4
Convergence rate for various time-stepping schemes for the Manufactured flow and arbitrary mesh motions.

MMS	Conservative formulation (8)		Non-conservative formulation (7)	
	L_2-pressure	H^1-energy	L_2-pressure	H^1-energy
Crank–Nicholson	2	2	1	1
IRK3	2	3	1	1
IRK5	3	5	1	1

Figs. 6 and 7 show temporal convergence rates for the manufactured solution in terms of H^1 norm of the velocity and L_2 norm of pressure. Convergence rate of the non-conservative formulation deteriorates to first order for both velocity and pressure as the time step is reduced. The conservative formulation delivers optimal rates of convergence for velocity and pressure as the time step is reduced (see Table 4).

9. Discussion

Tables 5–7 summarize results from all tests for the Crank–Nicholson, IRK3 and IRK5 time integrators.

The general conclusion is that the conservative formulation with formulas (49) and (50) for IRK3 and IRK5 time-stepping schemes and (51) and (52) for the Crank–Nicholson scheme yield the fixed mesh temporal accuracy on deforming meshes, thus satisfying the GCL at level 3. The non-conservative formulation with formulas (50) for IRK3 and IRK5 time-stepping schemes and (52) will yield only first order time accuracy on deforming meshes whereas optimal rates of convergence are observed on fixed grids. Other methodologies may improve the temporal convergence rate with the non-conservative formulation. This most often proves to be very expensive as many more evaluations of the residuals are required within a time-step than those prescribed by the time integrator. This has been done up to 2nd order time accuracy (see [3,4]). However the literature does not report such results for time integrators with temporal accuracy greater than 2.

The Taylor–Hood element used in the simulations has quadratic velocity interpolation and linear pressure approximation. Hence, it reproduces exactly the uniform, the Couette and Poiseuille flows on fixed meshes. This eliminates the space

Table 5
Convergence rate for various flows using non-conservative and conservative formulations with the Crank–Nicholson scheme.

Test flow	Conservative formulation		Non-conservative formulation	
	L_2-pressure	H^1-energy	L_2-pressure	H^1-energy
Uniform	Exact	Exact	Exact	Exact
Couette (1D motion)	Exact	Exact	1	1
Couette (2D motion)	2	2	1	1
Poiseuille (2D motion)	2	2	1	1
MMS	2	2	1	1

Table 6
Convergence rate for various flows using non-conservative and conservative formulations with IRK3 integrator.

Test flow	Conservative formulation		Non-conservative formulation	
	L_2-pressure	H^1-energy	L_2-pressure	H^1-energy
Uniform	Exact	Exact	Exact	Exact
Couette (1D motion)	2	3	1	1
Couette (2D motion)	2	3	1	1
Poiseuille (2D motion)	2	3	1	1
MMS	2	3	1	1

Table 7
Convergence rate for various flows using non-conservative and conservative formulations with the IRK5 integrator.

Test flow	Conservative formulation		Non-conservative formulation	
	L_2-pressure	H^1-energy	L_2-pressure	H^1-energy
Uniform	Exact	Exact	Exact	Exact
Couette (1D motion)	3	5	1	1
Poiseuille (2D motion)	3	5	1	1
MMS	3	5	1	1

discretisation errors so that the solution accuracy is only affected by GCL compliance and time accuracy and allows an analytical time truncation analysis. Thorough numerical tests were reported along with analytical studies of the Crank–Nicholson and IRK3 schemes explaining the observed behaviour.

Remark: Our work shows that one way to achieve GCL compliance and optimal time accuracy for a given time integrator is to evaluate the divergence of the mesh velocity, and the mesh velocity separately as if there were two mesh velocities: $\mathbf{v}_d$ to evaluate $(\nabla \cdot \mathbf{v}_d)$ and $\mathbf{v}_m$.

From our study of the three time integrators used in this paper, we conclude that the proposed methodology to construct mesh velocity divergence and mesh velocities should be applicable to a significant portion (if not the majority) of time integrators in a straight forward manner independently of space dimension.

10. Conclusions

This paper presented a new approach for constructing GCL compliant time accurate ALE finite element methods for viscous incompressible flows. The approach consists in decoupling the construction of the mesh velocity divergence $(\nabla \cdot \mathbf{v}_d)$ from the construction of the mesh velocity itself $\mathbf{v}_m$. This provides the flexibility to achieve GCL compliance and to maintain the temporal accuracy of the fixed mesh time-integrator when applied to flows on deforming domains. The approach is applicable to a broad spectrum of time integrators ranging from the commonly used first order implicit backward Euler scheme through the very popular second order Crank–Nicholson scheme to more sophisticated 3rd and 5th order Implicit Runge–Kutta schemes.

Analytical solutions and numerical grid and time step refinement studies were used to determine under what conditions the conservative and non-conservative weak forms of the Navier–Stokes equations satisfy the GCL and maintain (or not) the fixed mesh high order temporal accuracy of the time integrator when applied to flows on deforming domains.

We show that the GCL compliant non-conservative formulation is of order one in time. The examples studied, though, indicate that their temporal accuracy is closest to first order.

For the conservative formulation, construction of the mesh velocity divergence determines GCL compliance while the method for evaluating the mesh velocity is responsible for maintaining the high order temporal accuracy of the fixed mesh time integrator when used on deforming meshes (GCL, level 3).

Formal proofs are given that the formulas for the mesh velocity divergence guarantees GCL and DGCL compliance on deforming meshes of linear straight-sided triangular or tetrahedral elements. Proof is also given that the mesh velocity itself guarantees that the fixed mesh temporal accuracy is retained on meshes of deforming straight-sided triangles and tetrahedra.

The formulas developed in this work are straight forward to implement, result in simpler codes that are easier to modify and maintain because the same time-integrator can be used for two- or three-dimensional flows and for fixed and deforming domains.

Optimal temporal accuracy on deforming domains was demonstrated analytically on simple flows and confirmed by thorough time-step and mesh refinement studies.

A manufactured solution exercising all terms of the Navier–Stokes equations, provided quantitative data confirming the validity and properties of the proposed methodology for more complex flows.

Some aspects of the GCL remain to be investigated. While a successful approach was presented for deriving an appropriate mesh velocity divergence, the issue of reconstructing a mesh velocity field $\mathbf{v}_m$ from a GCL compliant field of $(\nabla \cdot \mathbf{v}_d)$ remains an open question.

The question of stability of schemes has not been addressed for the formulations presented here. Previous studies indicate that the GCL may not be related to stability but that it may enhance and/or suppress oscillations. The present approach might lead to good stability properties. In fact it might inherit some of the stability properties of the fixed mesh integrator since it uses the same integrator on fixed and deforming meshes. However, this remains to be confirmed.

Finally, even if our analytical error analysis holds in 3D, optimal accuracy remains to be confirmed by numerical tests on a 3D manufactured solution.

Acknowledgements

This work was sponsored in part by NSERC (Government of Canada) and the Canada Research Chair Program (Government of Canada).

Appendix A. Iterated Richardson extrapolation

Consider an unsteady flow simulation of accuracy $\mathcal{O}(h^p, \delta^n)$ with p the spatial accuracy and n the temporal order of accuracy. We call this the baseline solution. Consider now the baseline solution $u(h,\delta)$ and a sequence of approximate solutions generated by successively halving the time step δ and a solution for which the time-step is reduced to zero $u(h,0)$. Given approximate solutions $u(h,\delta/2^i)$, $i \in [0, N-1]$, with temporal accuracy of order n to an exact solution u_{exa}. We have

$$u(h,0) = u(h,\delta/2^i) + c_n(h)\left(\frac{\delta}{2^i}\right)^n + c_{n+1}(h)\left(\frac{\delta}{2^i}\right)^{n+1} + c_{n+2}(h)\left(\frac{\delta}{2^i}\right)^{n+2} + \mathcal{O}\left[\left(\frac{\delta}{2^i}\right)^{n+3}\right], \quad i \in [0, N-1] \tag{A.1}$$

We use Richardson extrapolation to eliminate error terms at order n between the two successive approximations $u(h,\delta/2^i)$ and $u(h,\delta/2^{i+1})$ to obtain more precise approximate solutions.

$$u(h,0) = \frac{2^n u(h,\delta/2^i) - u(h,\delta/2^{i+1})}{2^n - 1} - \frac{c_{n+1}(h)}{2(2^n-1)}\left(\frac{\delta}{2^i}\right)^{n+1} - \frac{3c_{n+2}(h)}{4(2^n-1)}\left(\frac{\delta}{2^i}\right)^{n+2} + \mathcal{O}\left[\left(\frac{\delta}{2^i}\right)^{n+3}\right], \quad i \in [0, N-2] \tag{A.2}$$

We define the first Richardson extrapolated approximations to $u(h,0)$ as u^1

$$u^1(h,\delta/2^i) = \frac{2^n u(h,\delta/2^i) - u(h,\delta/2^{i+1})}{2^n - 1}, \quad i \in [0, N-2] \tag{A.3}$$

We repeat the Richardson extrapolation on u^1 to obtain the 2^{nd} Richardson extrapolated approximation u^2 to $u(h,0)$ until we are left with u^{N-1}, the so-called iterated Richardson extrapolation:

$$\begin{aligned} u(h,0) - u^{N-1}(h,\delta) &= \frac{\prod_{i=1}^{N-1}(2^i - 1)c_{n+N-1}(h)}{\prod_{i=1}^{N-1} 2^i \prod_{i=1}^{N-1}(2^{n+i-1} - 1)}\delta^{n+N-1} + \mathcal{O}\left[\frac{\delta^{n+N}}{2^{(N-1)(n+N/2-1)}}\right] \\ u(h,0) - u^{N-1}(h,\delta) &\simeq 0.3c_{n+N-1}(h)\left(\frac{\delta}{2^{N-1}}\right)^n \left(\frac{\delta}{2^{(N-2)/2}}\right)^{N-1} \end{aligned} \tag{A.4}$$

which has a much better order of accuracy than that of the leading error term of the initial approximate solution for the smallest time-step

$$u(h,0) - u(h,\delta/2^{N-1}) = c_n(h)\left(\frac{\delta}{2^{N-1}}\right)^n + \mathcal{O}[(\delta/2^N)^{n+1}] \tag{A.5}$$

References

[1] J.G. Trulio, K.R. Trigger, Numerical solution of the one-dimensional hydrodynamic equations in an arbitrary time-dpendent coordinate system, Technical Report UCLR-6522, University of California Lawrence Radiation laboratory, 1961.

[2] C. Farhat, C. Degand, B. Koobus, M. Lesoinne, Torsional springs for two-dimensional dynamic unstructured fluid meshes, Computer Methods in Applied Mechanical Engineering 163 (1998) 231–245.

[3] L. Formaggia, F. Nobile, Stability analysis of second-order time accurate schemes for ale-fem, Computer Methods in Applied Mechanics and Engineering 193 (2004) 4097–4116.

[4] M. Lesoinne, C. Farhat, Geometric conservation laws for flow problems with moving boundaries and deformable meshes, and their impact on aeroelastic computations, Computer Methods in Applied Mechanics and Engineering 134 (1996) 71–90.

[5] H. Guillard, C. Farhat, On the significance of the geometric conservation law for flow computations on moving meshes, Computer Methods in Applied Mechanical Engineering 190 (2000) 1467–1482.

[6] R. Kamakoti, W. Shyy, Evaluation of geometric conservation law using pressure-based fluid solver and moving grid technique, International Journal of Numerical Methods for Heat and Fluid Flow 14 (7) (2003) 851–865.

[7] B. Koobus, C. Farhat, Second-order time accurate and geometrically conservative implicit schemes for flow computations on unstructured dynamic meshes, Computer Methods in Applied Mechanics and Engineering 170 (1999) 103–129.

[8] H. Zhang, M. Reggio, J.Y. Trepanier, R. Camarero, Discrete form of the gcl and its implementation in cfd codes, Computers and fluids 22 (1993) 9–23.

[9] W. Shyy, H.S. Udaykumar, M.M. Rao, R.W. Smith, Computational fluid dynamics with moving boundaries, Computer Methods in Applied Mechanics and Engineering 193 (2004) 2019–2032.

[10] D. N'Dri, A. Garon, A. Fortin, Incompressible Navier–Stokes computations with stable and stabilized space–time formulations: a comparative study, Communications in Numerical Methods in Engineering 18 (2002) 495–512.

[11] X.D. Li, N.-E. Wiberg, Implementation and adaptivity of a space–time finite element method for structural dynamics, Computer Methods in Applied Mechanics and Engineering (1998) 156.

[12] P. Hansbo, J. Hermansson, T. Svedberg, Nitsche's method combined with space–time finite elements for ale fluid–structure interaction problems, Computer Methods in Applied Mechanical Engineering 193 (2004) 4195–4206.

[13] K. Stein, T.E. Tezduyar, R. Benney, Automatic mesh update with the solid-extension mesh moving technique, Computer Methods in Applied Mechanics and Engineering 193 (2004) 2019–2032.

[14] M. Lacroix, A. Garon, Numerical solution of phase change problems: an Eulerian–Lagrangian approach, Numerical Heat Transfer, Part B 19 (1992) 57–78.

[15] P.D. Thomas, C.K. Lombard, Geometric conservation law and its application to flow computations on moving grids, AIAA Journal (1979) 1030–1037.

[16] I. Demirdzic, M. Per8c, Space conservation law in finite volume calculation sof fluid flow, International Journal for Numerical Methods in Fluids 8 (1988) 1037–1050.

[17] L. Formaggia, F. Nobile, A stability analysis for the arbitrary lagrangian eulerian formulation with finite elements, East-West Journal of Numerical Mathematics 7 (1999) 105–131.

[18] B. Nkonga, On the conservative and accurate cfd approximations for moving meshes and moving boundaries, Computer Methods in Applied Mechanics and Engineering 190 (2000) 1801–1825.

[19] C. Farhat, P. Geuzainne, C. Grandmont, The discrete geometric conservation law and the nonlinear stability of ale schemes for the solution of flow problems on moving grids, Journal of Computational Physics 174 (2001) 669–694.

[20] W. Cao, W. Huang, R.D. Russell, A moving mesh method based on the geometric conservation law SIAM Journal of Scientific Computing 24 (2002) 118–142.

[21] R.E. Gordnier, R. Fithen, Coupling of a nonlinear finite element structural method with a Navier–Stokes solver, Computers and Structure 81 (2003) 75–89.

[22] Y. Lian, W. Shyy, D. Viieru, B. Zhang, Membrane wing aerodynamics for micro air vehicles, Progress in Aerospace Sciences (2003) 39.

[23] D. Boffi, L. Gastaldi, Stability and geometric conservation laws for ale formulations, Computer Methods in Applied Mechanical Engineering 193 (2004) 4717–4739.

[24] Y.J. Jan, T.W.-H. Sheu, Finite element analysis of vortex sheding oscillations from cylinders in the straight channel, Computational Mechanics 33 (2004) 81–94.

[25] C. Grandmont, P. Geuzaine, F. Farhat, Design and analysis of ale schemes with provable second-order time-accuracy for inviscid and viscous flow simulations, Journal of Computaional Physics 191 (2003) 206–227.

[26] D.J. Mavriplis, Z. Yang. Achieving higher-order time accuracy for dynamic unstructured mesh fluid flow simulations: role of the gcl, in: 17th AIAA Fluid Dynamic Conference, Toronto, Ontario, June 2005, AIAA Paper 2005-5114.

[27] M. Engel, M. Griebel, Flow simulation on moving boundary-fitted grids and application to fluid–structure interaction problems, International Journal for Numerical Methods in Fluids 50 (2006) 437–468.

[28] C. Förster, W.A. Wall, E. Ramm, On the geometric conservation law in transient flow calculations on deforming domains, International Journal for Numerical Methods in Fluids 50 (2006) 1369–1379.

[29] H. Schlichting, Boundary-Layer Theory, 7th ed., McGraw-Hill, 1979.

[30] M. Heil, Stokes flow in an elastic tube – a large-displacement fluid–structure interaction problem, Journal for Numerical Methods in Fluids 28 (1998) 243–265.

[31] C. Degand, C. Farhat, A three-dimensional torsional spring analogy method for unstructured dynamic meshes, Computers and Structures 80 (2001) 05–316.

[32] P.A. Sackinger, P.R. Schunk, R.R. Rao, A Newton–Raphson pseudo-solid domain mapping technique for free and moving boundary problems: a finite element implementation, Journal of Computational Physics 125 (1996) 83–103.

[33] H. Moller, E. Lund. Shape sensitivity analysis of strongly coupled fluid–structure interaction problems, in: 8th AIAA/NASA/USAF/ISSMO Symposium on Multidisciplinary Analysis and Optimization, Long Beach, California, September 2000, AIAA Paper 2000-4823.

[34] R. Lohner, C. Yang, Improved ale mesh velocities for moving bodies, Communications in Numerical Methods in Engineering 12 (1996) 599–608.

[35] E. Lund, H. Moller, L.A. Jakobsen. Shape design optimization of steady fluid–structure interaction problems with large displacements, in: 42nd AIAA/ASME/ASCE/AHS/ASC Structures, Structural Dynamics, and Materials Conference and Exhibit, Seattle, Washington, April 2001, AIAA Paper 2001-1624.

[36] E. Lund, H. Moller, L.A. Jakobsen, Shape design optimization of stationary fluid–structure interaction problems with large displacements and turbulence, Structural and Multidisciplinary Optimization 25 (2003) 383–392.

[37] G. Chiandussi, G. Bugeda, E. Oñate, A simple method for automatic update of finite element meshes, Communications in Numerical Methods in Engineering 16 (2000) 1–19.

[38] E. Oñate, J. Garcia, A finite element method for fluid–structure interaction with surface waves using a finite calculus formulation, Computer Methods in Applied Mechanical Engineering 191 (2001) 635–660.

[39] E.J. Nielsen, W.K. Anderson, Recent improvements in aerodynamic design optimization on unstructured meshes, in: 39th AIAA Aerospace Science Meeting, Reno, Nevada, January 2001, AIAA Paper 2001-0596.

[40] S. Etienne, D. Pelletier, A monolithic formulation for steady-state fluid–structure interaction problems, in: 34th AIAA Fluid Dynamics Conference and Exhibit, Portland, Oregon, June 2004, AIAA Paper 2004-2239.

[41] O. Schenk, K. GSrtner, Solving unsymmetric sparse systems of linear equations with pardiso, Journal of Future Generation Computer Systems 20 (3) (2004) 475–487.

[42] O. Schenk, K. Gärtner, On fast factorization pivoting methods for symmetric indefinite systems, Electronic Transactions on Numerical Analysis 23 (2006) 158–179.

[43] E. Hairer, G. Wanner, Solving Ordinary Differential Equations II, 2nd revised ed., Stiff and Differential-Algebraic Problems, Springer, Germany, 2002.

[44] P.J. Roache, Verification and Validation in Computational Science and Engineering, Hermosa Publishers, Albuquerque, New Mexico, 1998.

[45] A. Fortin. Analyse numérique pour ingénieurs, Éditions de l'École Polytechnique de Montréal, Montréal, Québec, 1995.